SCIENTIFIC REPORTS

OPEN

CONFERENCE PROCEEDINGS

APEnergy2014

SUBJECT AREAS:
COMPOSITES
BATTERIES

Received
28 February 2014

Accepted
9 April 2014

Published
29 August 2014

Correspondence and requests for materials should be addressed to H.X.J. (jihengx@ustc.edu.cn) or Y.W.Z. (zhuyanwu@ustc.edu.cn)

Manipulating Size of $Li_3V_2(PO_4)_3$ with Reduced Graphene Oxide: towards High-Performance Composite Cathode for Lithium Ion Batteries

Xianjun Zhu[1], Zan Yan[1], Wenyan Wu[1], Wencong Zeng[2], Yuanxin Du[2], Yu Zhong[1], Haidie Zhai[1], Hengxing Ji[2] & Yanwu Zhu[2]

[1]College of Chemistry, Central China Normal University, 152 Luoyu Rd, Wuhan, Hubei 430079 (P. R. China), [2]Department of Materials Science and Engineering & CAS Key Laboratory of Materials for Energy Conversion, University of Science and Technology of China, 96 Jin Zhai Rd, Hefei, Anhui 230026 (P. R. China).

Lithium vanadium phosphate ($Li_3V_2(PO_4)_3$, LVP)/reduced graphene oxide (rGO) composite is prepared with a rheological method followed by heat treatment. The size and interface of LVP particles, two important merits for a cathode material, can be effectively tuned by the rGO in the composite, which plays as surfactant to assist sol-gelation and simultaneously as conductive carbon coating. As a consequence, the composite with 7.0 ± 0.4 wt.% rGO shows a capacity of 141.6 mAh g^{-1} at 0.075 C, and a rate capacity of 119.0 mAh g^{-1} at 15 C with respect to the mass of LVP/rGO composite, and an excellent cycling stability that retains 98.7% of the initial discharge capacity after 50 cycles. The improved electrochemical performance is attributed to the well-controlled rGO content that yields synergic effects between LVP and rGO. Not only do the rGO sheets reduce the size of LVP particles that favor the Li^+ ion migration and the electron transfer during charging and discharging, but also contribute to the reversible lithium ions storage.

Lithium ion battery is considered as one of the most efficient energy storage system for its high energy density and long lifetime, which is highly demanded for energy storage, such as electric vehicles (EVs)[1,2]. However, the energy density and power density of lithium ion batteries are still below 200 Wh kg^{-1} and 400 W kg^{-1}, respectively, mainly due to the low specific capacity and poor rate capability of cathode materials. Phosphate cathode materials are safe and environmentally friendly compared to spinel lithium manganese oxide ($LiMn_2O_4$) and layered lithium cobalt oxide ($LiCoO_2$)[3]. With a theoretical specific capacity of 197 mAh g^{-1}, the highest value among those of phosphate cathode materials, monoclinic lithium vanadium phosphate ($Li_3V_2(PO_4)_3$, LVP) is a promising cathode material candidate for lithium ion batteries. In practice, however, the specific capacity which one can achieve for LVP is usually lower than 132 mAh g^{-1}, by extracting 2 moles Li^+ ions out of 1 mole LVP in the potential range of 3 ~ 4.3 V based on the V^{3+}/V^{4+} redox couple[4–6]. When the third Li^+ ions are extracted in the wider voltage window (3 ~ 4.8 V), the specific capacity of LVP fades rapidly as a result of $V_2(PO_4)_3$ structural instability and side reactions between electrolyte and $Li_xV_2(PO_4)_3$ ($0 \le x \le 3.0$) at a high voltage of 4.8 V[7,8]. On the other hand, the poor electric conductivity of LVP (2.4×10^{-7} s cm^{-1}) has largely limited its power density[9]. Therefore, cation doping[10], reducing size of LVP particles[11] and carbon coating[12] are usually necessary to improve the Li^+ ion insertion/extraction kinetics.

In recent studies, graphene shows excellent electric conductivity, remarkable structural flexibility, and high mechanical/electrochemical stability[13–15]. Graphene can improve the specific capacity and rate capability of the cathode when it is mixed with electrochemically active materials. For example, Zhang et al.[6] and Liu et al.[16] reported the enhanced rate capability of LVP, in which, the uniform dispersion and coverage of graphene sheets on electrochemically active materials is the key because the solid/liquid interface can be effectively modified with minimized use of graphene. The particle size and surface properties of LVP are two of the most important parameters that affect the electrochemical properties[11,17,18]. It is critical to understand the effect of graphene on the electrochemical performance of olivine-structure materials. Especially, recent progress in mass production of reduced graphene oxide (rGO) greatly reduces the cost of graphene-based materials; consequently, this would make it possible for the outstanding properties of graphene found in laboratory to be applied in industry[19]. To

meet this goal, it is highly desired to have a facile method with moderate synthesis conditions, well-controlled product uniformity and high reproducibility.

Herein we report a rheological approach to synthesis of LVP/rGO composites. The LVP particles are uniformly enwrapped and distributed on the surface of rGO, and simultaneously the rGO sheets form an interconnected conducting scaffold for the excellent electron conduction between LVP particles. We found that rGO sheets play as a surfactant that limits the size of LVP particles, a highly conducive carbon coating, and an additional medium for Li^+ ions storage in the potential range of 2 ~ 4.2 V. Consequently, the LVP/rGO composite with an optimum rGO content of 7.0 ± 0.4 wt.% delivers an improved specific capacity and a high rate capability. We obtain a specific capacity of 141.6 mAh g^{-1} and a rate capacity of 119.0 mAh g^{-1} at 15 C based on the mass of LVP/rGO composite at the current density of 0.075 C (1 C = 132 mAh g^{-1}) (152.3 mAh g^{-1} at 0.075 C and 128.0 mAh g^{-1} at 15 C based on the mass of LVP). The specific capacity is higher than the theoretical value of 132 mAh g^{-1} for pure LVP by extracting/inserting 2 Li^+ ions in LVP in the potential range of 2 to 4.2 V. The contribution of rGO to Li^+ ions storage in the LVP/rGO composites with rGO content of 3.1 ± 0.3, 7.0 ± 0.4, 20.0 ± 0.5 and 29.9 ± 0.5 wt.% are qualitatively deduced, indicating that a rational control of rGO content is a key in tuning the morphology of rGO-enwrapped LVP for improved performance.

Results

As shown in Fig. 1a, graphite oxide prepared by a modified Hummers' method, was sonicated in water to form a suspension of graphene oxide (GO) platelets. For the synthesis of the LVP/rGO composite, NH_4VO_3, $LiOH{\cdot}H_2O$ and $NH_4H_2PO_4$ solutions were slowly and sequentially added to the GO suspension under stirring. After being exposed to ultrasound in an ultrasonic bath, the mixture was heated under stirring to become a sol-gel during the rheological process. When being cooled to room temperature, the sol-gel was pre-annealed at 400°C for 4 h in a reduced atmosphere of Ar and H_2 mixture (1 : 0.05 by volume). Finally, the LVP/rGO composite was obtained by annealing the pre-dried sol-gel at 800°C for 8 h at the same atmosphere. During the procedures, GO was converted to rGO. The content of rGO in the final LVP/rGO composite was determined by chemical method. The scanning electron microscopy (SEM) images of the GO (Fig. 1b), pre-annealed sol-gel (Fig. 1c) and final LVP/rGO composite with 7.0 ± 0.4 wt.% rGO (Fig. 1d) are shown below each step of the preparation, respectively. It can be seen that the LVP particles are closely wrapped by wrinkled rGO sheets in the composite, which is further confirmed by the transmission electron microscopy (TEM) image of LVP/rGO in Fig. 1e. The high-resolution TEM image in Fig. 1f highlights the atomically sharp interface between LVP and rGO, and the high crystallinity of LVP crystals, which is also supported by the selected area electron diffraction pattern in the inset of Fig. 1f. In the XRD patterns of the LVP/rGO composites shown in Fig. S1, all diffraction peaks have been identified as the monoclinic LVP structure with space group of $P_{21/n}$ (JCPDS No. 97-009-6962). The absence of graphene diffraction peaks in the composites might be due to the relatively low content and well-exfoliated form of rGO in the samples. Raman spectroscopy for the LVP/7.0 ± 0.4 wt.%rGO composite (Fig. 1g) confirms the presence of rGO in the composite. The intensity ratio of D (~1349.7 cm^{-1}) to G (~1602.6 cm^{-1}) band (I_D/I_G) is about 1.38; it was claimed that a high degree of disordering in carbon might favor its good electrochemical properties[4]. The X-ray photoelectron spectroscopy (XPS) C1s spectrum (Fig. S2) suggests that oxygen-containing functional groups (e.g. C-OH, C=O and O=C-OH) are present in the LVP/rGO composite.

The average size of LVP particles in the composite has been tuned with the rGO content, as shown in the SEM images in Fig. 2a–e. Being calculated from the size distribution of LVP particles (Fig. S3) in the composites with rGO contents of 0 wt.%, 3.1 ± 0.3 wt.%, 7.0 ± 0.4 wt.% 20.0 ± 0.5 wt.% and 29.9 ± 0.5 wt.%, respectively, the average size of LVP particles shows a monotonous decrease with the content of rGO, as shown in Fig. 2f. This result is in consistence with the broadened and decreased XRD characteristic peaks of LVP (Fig. S1) for the composites with higher rGO contents. In addition, the shape of LVP particles gradually transforms from dumbbell-like to spherical during the reduction of size. Therefore the dispersed GO sheets effectively serve as a surfactant preventing the aggregation of LVP during drying and annealing. Such a role of GO sheets is assured by the good dispersion of GO platelets which are negatively charged, especially in basic solution mixture of NH_4VO_3, $LiOH{\cdot}H_2O$ and $NH_4H_2PO_4$ (pH ~ 9). Here, GO plays as a similar role as citric acid that is widely used in synthesizing carbon coated phosphate, e.g. LVP nanoparticles[20]. In the sol-gel process for preparation of LVP, the citric acid acts as a surfactant template suppressing the LVP particles size. After annealing, the citric acid is also a source of amorphous carbon coated on the LVP surface. In comparison, rGO as a product of GO upon annealing is mostly sp^2 hybridized carbon, more conductive and more stable than amorphous carbon. Thus the replacement of citric acid or other organic molecules with GO for sol-gel may be favorable for the following electrochemical reactions.

Fig. 3a shows the cyclic voltammetry curves of the LVP/rGO composite with 7.0 ± 0.4 wt.% rGO content at a scan rate of 0.1 mV/s in the potential range of 2.0 ~ 4.2 V. Three couples of oxidation and reduction peaks were observed. In the anodic direction, the first

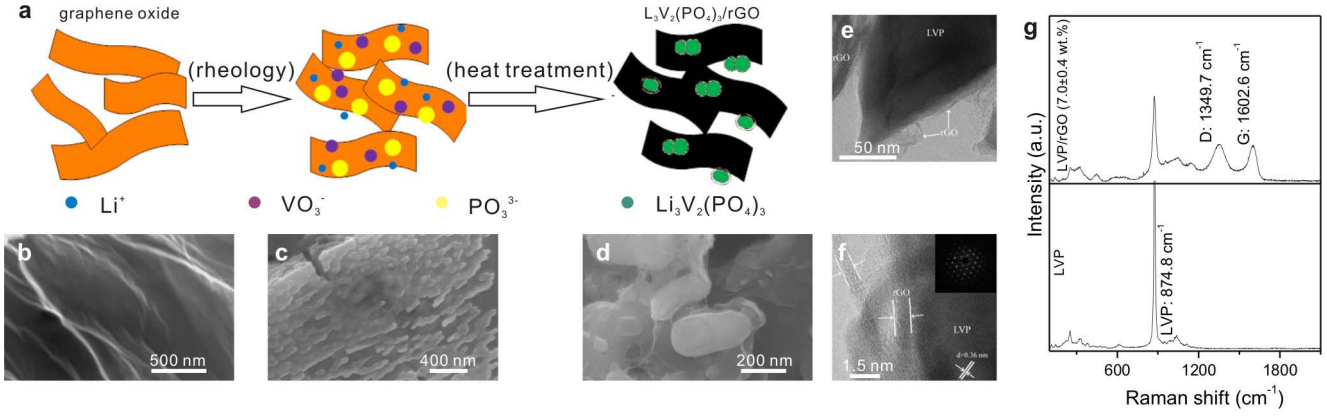

Figure 1 | LVP/rGO composite preparation and morphology. (a) Scheme of the synthesis process. (b–d) Typical SEM images of products from each step are shown below the schematic. (e) Typical TEM and (f) HRTEM images of the composite with 7.0 ± 0.4 wt.% rGO. (g) Raman spectra of composite with 7.0 ± 0.4 wt.% rGO and pure LVP.

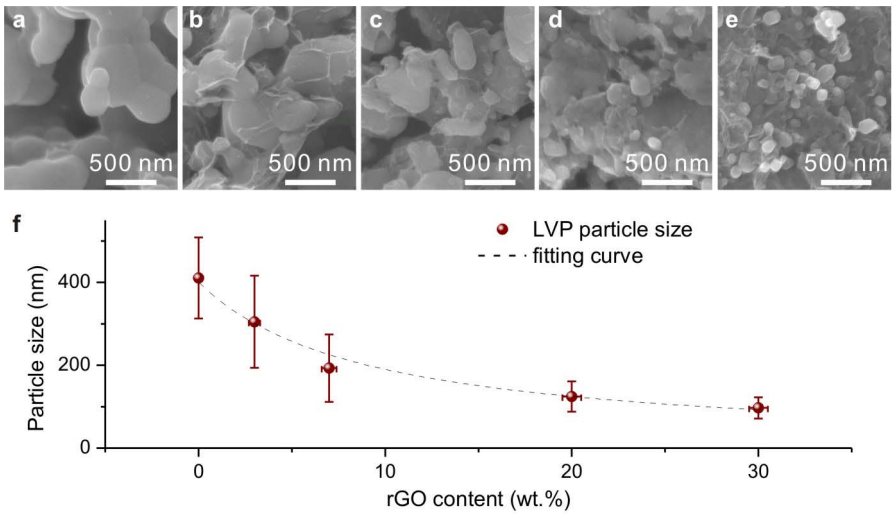

Figure 2 | SEM images of LVP with different contents of rGO. (a) Pure LVP, (b) 3.1 ± 0.3 wt.%, (c) 7.0 ± 0.4 wt.%, (d) 20.0 ± 0.5 wt.%, (e) 29.9 ± 0.5 wt.%, and (f) The particle size of LVP dependent on the content of rGO in the composites.

lithium is removed at 3.62 and 3.69 V, and the second lithium is extracted at 4.11 V; in the cathode direction, the corresponding three reduction peaks are located at 3.55, 3.64, and 4.02 V, indicating that 2 Li^+ ions per LVP molecule are inserted and extracted reversibly. The initial charging/discharging curves of the composite at the rate of 0.075 C in the potential window of 2.0 ~ 4.2 V are shown in Fig. 3b. When the composite is charged to 4.2 V, three flat plateaus at 3.60, 3.69 and 4.08 V correspond to different charging stages of $Li_xV_2(PO_4)_3$ at $x = 3.0, 2.5, 2.0$ and 1.0, respectively[17]. The composite with 7.0 ± 0.4 wt.% rGO delivers a specific capacity of 133.5 and 141.6 mAh g^{-1} in the first charge and discharge, respectively, with respect to the total mass of the LVP/rGO composite (143.5 and

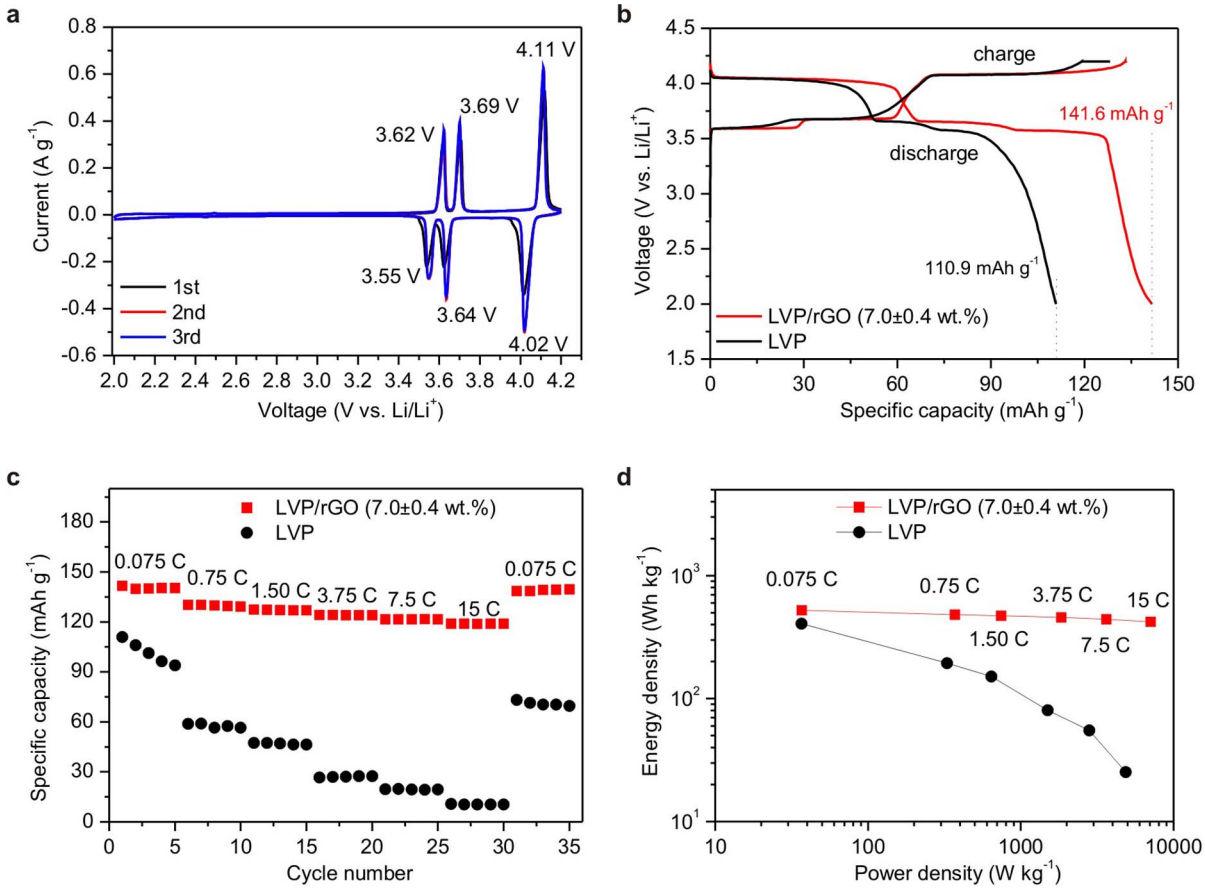

Figure 3 | (a) Cyclic voltammetry curves of the composite with 7.0 ± 0.4 wt.% rGO at a scan rate of 0.1 mV/s in the potential range of 2.0 ~ 4.2 V. (b) The initial charge/discharge profiles of pure LVP and the composite with 7.0 ± 0.4 wt.% rGO at the current density of 0.075 C. (c) Rate performance of the composite with 7.0 ± 0.4 wt.% rGO at various current densities. (d) Ragone plot correlating the gravimetric densities of energy and power of LVP/rGO|Li half cells containing 1 M $LiPF_6$ in EC and DEC (1 : 1 by volume).

152.3 mAh g^{-1}, respectively, based on the mass of LVP in the composite). In comparison, pure LVP delivers specific capacities of 128.2 and 110.9 mAh g^{-1} for the first charge and discharge, respectively. The initial coulombic efficiency of the LVP/rGO composite (discharge to charge) is 106.1%, higher than 86.5% of the coulombic efficiency measured for pure LVP cathode. Furthermore, the first discharge capacity of 141.6 mAh g^{-1} for the LVP/rGO is 7.3%, higher than the theoretical value of 132 mAh g^{-1} for pure LVP that was calculated by extracting/inserting 2 Li^+ ions below the voltage of 4.2 V; to the best of our knowledge, it is the highest value among those previously reported in the literatures[11,16,18,21]. Long-term charging and discharging cycling for the composite with 7.0 ± 0.4 wt.% rGO at the rate of 0.075 C (Fig. S4) shows that the composite still delivers a high specific capacity of 139.8 mAh g^{-1} (98.7% retention) after 50 cycles and the coulombic efficiency is in the range of 96 ~ 98% since the second cycle. As a comparison, the capacity of pure LVP decreases from 110.9 mAh g^{-1} of the first discharge capacity to 62.1 mAh g^{-1} on the 50th cycle, with a retention of only 56.0%.

Fig. 3c shows the rate performance of LVP/rGO with 7.0 ± 0.4 wt.% rGO content at different current densities. With the increase in the current density from 0.075 to 15 C, the discharge capacity decreases from 141.6 to 119.0 mAh g^{-1} (84.0% retention). This capacity is significantly higher than ~10 mAh g^{-1} of pure LVP measured at 15 C. The rate performance presented here is also much better than those previously reported, such as nanostructured LVP/carbon (125.4 mAh g^{-1} at 5 C)[11], LVP/graphene (118 mAh g^{-1} at 5 C)[16], and nanocomposite LVP/graphene (110 mAh g^{-1} at 10 C)[21]. In addition, as long as the current reverts back to 0.075 C, the capacity of LVP/rGO is recovered to 138.5 mAh g^{-1}. At the same time, the coulombic efficiency of LVP/rGO maintains at 98 ~ 100% for various high current densities. After C-rate test, SEM study (Fig. S5) shows that the morphology of LVP particles in the LVP/rGO composite electrode experienced a change, indicating that the composite is tolerant to varied charge and discharge currents, which is highly desirable for electrode materials in lithium ion batteries. The Ragone plot in Fig. 3d further highlights the excellent rate performance of the composite with 7.0 ± 0.4 wt.% rGO in the rate range of from 0.075 to 15 C. Comparing to pure LVP, the relatively flat curve from the composite indicates that most of the energy stored in the material is available for utilization, less dependent on the power till 7000 W/kg (15 C). This property sheds light on rapid charge/discharge applications when the LVP/rGO composite is used in Li-ion batteries.

Discussion

It is well known that the major capacity of LVP is attributed to the Li^+ insertion into and extraction from the LVP particles. There are two major limiting processes reported to explain why some lithium ions cannot be fully extracted from the ordered-olivine structure which in turn causes capacity loss: (i) Limited lithium ion phase-boundary diffusion, where the Li^+ diffusion may be interrupted by ionic disorder, foreign phases or stacking faults; (ii) Low electronic conductivity, which may limit the Li^+ insertion/extraction since the total charges must be kept in balance during charging and discharging. In recent attempts to more efficient Li^+ diffusion in the olivine structure, the introduction of graphene has resulted in promising rate performances (e.g. 118 and 70 mAh g^{-1} at 5 and 50 C, respectively, in Ref. 16; 104, 91, and 85 mAh g^{-1} at 5, 30 and 50 C, respectively, in Ref. 6), while all published specific capacities are less than the theoretical value 132 mAh g^{-1} of LVP below the voltage of 4.2 V.

The enhanced capacity of the LVP/rGO composites in this work is considered to be associated with the addition of rGO sheets. To clarify the contribution from rGO, the galvanostatic charging/discharging data of LVP/rGO composites with the contents of 0, 3.1 ± 0.3, 7.0 ± 0.4, 20.0 ± 0.5, 29.9 ± 0.5 wt.% rGO were obtained at a rate of 0.075 C and the first charge/discharge curves are shown in Fig. 4a for comparison. As we can see, the specific capacity (normalized to composite mass) at the first discharge increases from 110.9 for pure LVP to the highest value of 141.6 mAh g^{-1} for the composite with 7.0 ± 0.4 wt.% rGO, then decreases with further increase in the content of rGO (Fig. 4b). At the same time the initial coulombic efficiency monotonously increases from 86.5% for pure LVP to 131.0% for the composite with 29.9 ± 0.5 wt.% rGO (Fig. 4b). In our previous study[22], the solid electrolyte interphase formation/decomposition for pure rGO takes place at the voltage of less than 2 V. There are no other faradic reactions occurring except for Li^+ ion insertion/extraction in LVP as shown in CV (Fig. 3a); thus we suggest that this capacity enhancement of LVP/rGO composite shown in Fig. 4a is ascribable to Li^+ ion adsorption/desorption on graphene sheets. In order to study the Li^+ storage contribution of rGO, we calculated the total capacities delivered in the first discharge curves (Fig. 4a) of LVP/rGO composites in the potential window of 2.0 ~ 3.0 V, in which neither Li^+ ion insertion in LVP nor solid electrolyte interphase formation/decomposition occurred (Fig. 3a), thus, can be assigned to Li^+ ions adsorption on rGO surface. The discharge curve of pure rGO in the voltage window of 2.0 ~ 4.2 V shows a linear voltage-specific capacity relationship (Fig. S6a), therefore, the capacities of rGO in the LVP/rGO composite in the potential window of 2.0 ~ 4.2 V can be estimated by taking the capacity value obtained in the potential window of 2.0 ~ 3.0 V multiplied with a factor of 2.2, and are shown in Fig. 4c as the function of rGO content. We can see that the highest capacity contributed from rGO was obtained from the composite with 3.1 ± 0.3 wt.% and with 7.0 ± 0.4 wt.% rGO. At a rGO content of 7.0 ± 0.4 wt.% in the composite, rGO delivers a specific capacity of 333.1 mAh g^{-1} per mass of rGO. Considering a theoretical capacity of 132 mAh g^{-1} for pure LVP, a paper-pen calculation yields a specific capacity of 146.1 mAh g^{-1} (132 × 0.93 + 333.1 × 0.07 = 146.1) with respect to the mass of the composite containing 7.0 ± 0.4 wt.% rGO, which is close to the experimental data (141.6 mAh g^{-1}, in Fig. 3b). Here, 7.0 ± 0.4 wt.% rGO in the LVP/rGO composite contributes about 16% of the entire Li^+ ion storage capacity. However, possibly due to too low rGO content and/or too big size of LVP particles in the composite with 3.1 ± 0.3 wt.% rGO, some LVP particles cannot be wrapped by rGO as shown in Fig. 2b. On the other hand, rGO sheets tend to aggregate or restack in the composites with higher rGO contents such as 20.0 ± 0.5 wt.% or 29.9 ± 0.5 wt.%, although the size of LVP particles is smaller and the wrapping is more complete in these two samples. That is, the synergic effect between LVP and rGO is optimized in the composite with 7.0 ± 0.4 wt.% rGO, leading to an optimized electrochemical performance in the composite. Such a synergic effect involves the size of LVP particles, the contribution of rGO to reversible Li^+ ions storage and the interface between LVP and rGO mostly decided by the wrapping. In contrast, pure rGO delivers a low capacity of about 85 mAh g^{-1} by calculation (Fig. 4c) in the voltage window of 2.0 ~ 4.2 V, which is close to the experimentally measured value shown in Fig. S6b. In addition, the measured specific capacity of pure rGO is lower at the early stage of long term cycling, indicating that the low specific capacity of pure rGO is very likely due to the aggregation or restacking.

On the other hand, conductive rGO sheets in the composites could serve as a fast path for electron migration during charging and discharging. Thus the electrons can spread onto the entire surface of LVP particles, leading to the improved kinetics and reversibility of the lithium insertion/extraction cycles. The electrochemical performance of the LVP/rGO composite with 7.0 ± 0.4 wt.% rGO at 0.075 C is compared with that of the pure LVP in a wider potential range of 2.0 and 4.7 V, as shown in Fig. 5a. The charging plateau observed at 4.55 V corresponds to the extraction of the third Li^+ ion, associated with the phase transition process from $LiV_2(PO_4)_3$ to $V_2(PO_4)_3$. With the presence of rGO, the voltage plateau for the third Li^+ extraction from LVP in the composite is longer than that of pure LVP, which may partially contribute to the high capacity of the

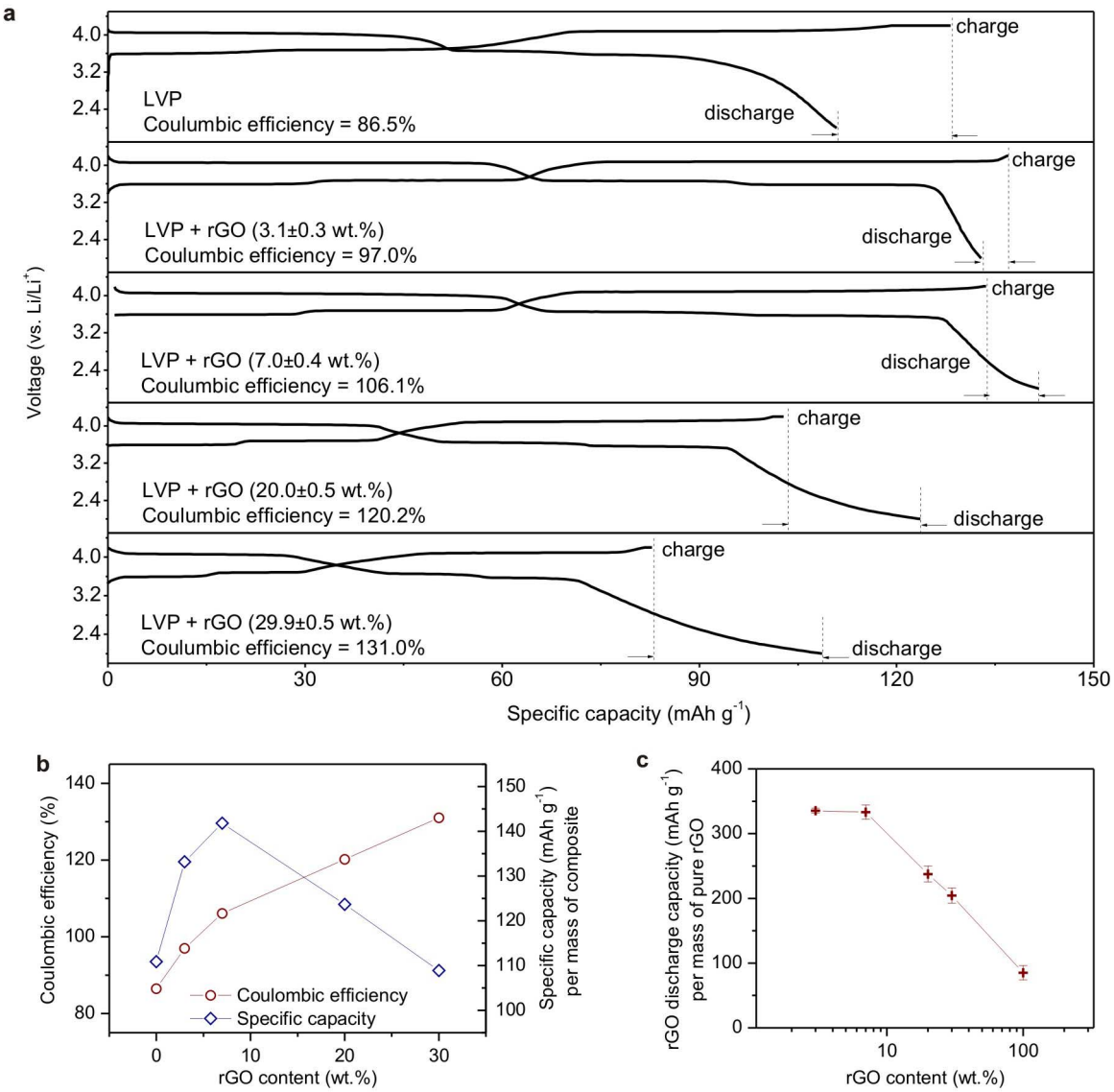

Figure 4 | (a) The first charge/discharge profiles of LVP/rGO composite at 0.075 C with different contents of rGO. (b) Coulombic efficiency of the composites and rGO specific capacity contribution in the composites dependent on the rGO content. (c) Specific capacity of rGO calculated from the initial discharge curves between 2.0 and 4.2 V as a function of rGO content.

composite. Cyclic voltammetry curve of the LVP/rGO composite shown in Fig. 5b demonstrates four oxidation peaks and three reduction peaks, corresponding to the relative extraction and reinsertion of Li^+. The absence of the third reduction peak agrees to the result of the initial reinsertion of Li^+ cation in $V_2(PO_4)_3$ from a solid solution of two phase[23]. Compared to the curve obtained from pure LVP, the well-defined and highly symmetrical peaks from the composite suggest that the enhancement of the electrochemical reversibility is related to the lower ohmic resistance in the electrode reactions due to the presence of the conductive rGO network in LVP/rGO composites.

In summary, the LVP/rGO composite has been prepared by a rheological method and the size of LVP particles in the composite was tuned with the content of rGO. By optimizing the synergic effect between LVP particles and rGO, the composite with 7.0 ± 0.4 wt.% rGO has demonstrated a high capacity of 141.6 mAh g^{-1} based on the mass of LVP/rGO composite (152.3 mAh g^{-1}, based on the mass of LVP), which is more than the theoretical capacity of 132 mAh g^{-1} for 2 Li^+ ions extraction/insertion below the voltage of 4.2 V in LVP, as well as a high rate capability of 119.0 mAh/g at 15 C and good cycling stability that retains 98.7% of the initial discharge capacity after 50 cycles. The contribution of rGO to the enhanced electrochemical performance has been argued based on the morphology and electrochemistry studies. We have demonstrated that, with a finely tuned rGO content rGO contributes to as high as 16% of the entire Li^+ ion storage capacity. The reduced LVP particle size favors Li^+ ion migration and the presence of graphene sheets improves electric conduction. Therefore, the LVP/rGO composite has a great potential as a cathode material for high-capacity and high C-rate lithium ion batteries.

Methods

Synthesis of graphite oxide. Graphite oxide was synthesized from natural graphite by a modified Hummers' method. Briefly, graphite powder (2 g; 500 mesh, Sinopharm Chemical Reagent Co., Ltd) and $NaNO_3$ (1 g; >99%) were mixed, then put into concentrated H_2SO_4 (96 ml; 98%) in an ice bath. Under vigorous stirring, $KMnO_4$ (6 g; 99.5%) was added gradually and the temperature of the mixture was kept below 20°C. After removing the ice bath, the mixture was stirred in a water bath at 35°C for 18 h. As the reaction progressed, the mixture became pasty with a brownish color. Successively, 150 ml H_2O was slowly added into the pasty mixture. Because adding water into the concentrated H_2SO_4 medium releases a large amount of heat, therefore water was slowly added and the temperature of the mixture should

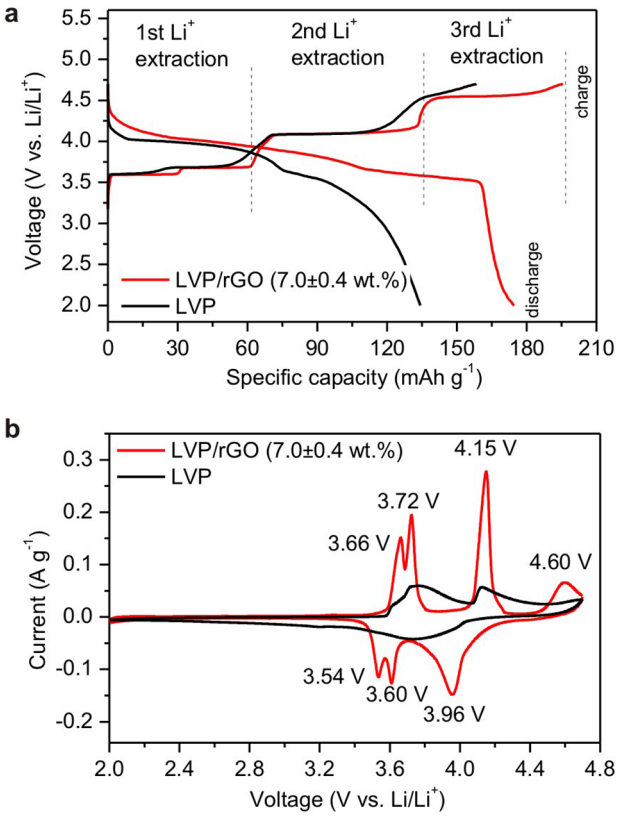

Figure 5 | (a) Initial charge/discharge profiles and (b) Cyclic voltammetry curves of pure LVP and LVP/(7.0 ± 0.4) wt.%rGO electrodes at a scan rate of 0.1 mV s^{-1}, in the voltage range of 2.0 ~ 4.7 V.

be kept below 50°C by putting it in the water bath. After diluting with 240 ml H_2O, 5 ml of 30% H_2O_2 (Sinopharm Chemical Reagent Co., Ltd) was added to the mixture, and the color of diluted solution was changed to brilliant yellow along with bubbling. After continuously stirring for another 2 h, the mixture was filtered and washed with HCl aqueous solution (250 ml, 1 : 1 by volume), DI water and ethanol to remove other ions. Finally, the resulting solid was dried by vacuum.

Preparation of LVP/rGO. The LVP/rGO was prepared by a rheological method and the following annealing. In a typical experiment, 4 mmol NH_4VO_3 (0.47 g; 99%), 6.2 mmol $LiOH{\cdot}H_2O$ (0.25 g; 99%) and 4 mmol $NH_4H_2PO_4$ (0.46 g; 99%) were separately dissolved in 10 ml water, respectively. NH_4VO_3, $LiOH{\cdot}H_2O$ and $NH_4H_2PO_4$ solutions were slowly and sequentially added to 100 ml GO suspension under stirring. After being exposed to ultrasound in an ultrasonic bath for 30 min, the mixture was heated at 80°C under stirring till water was mostly removed. When cooled to room temperature, the sol-gel was pre-annealed at 400°C for 4 h under an atmosphere of Ar + H_2 (1 : 0.05 by volume). Finally, the LVP/rGO was obtained by annealing the pre-annealed sol-gel at 800°C for 8 h at the same atmosphere.

The content of rGO in the LVP/rGO was identified by a chemical method. Typically, 200 mg LVP/rGO composite was added to 100 ml of HCl solution (3.7 wt.%) under stirring. When dissolving LVP in the composite completely, the suspension was filtered and washed by DI water several times. After being completely dried, the rGO residue was weighed.

Characterization. The structure of the as-prepared LVP/rGO was characterized by X-ray diffraction (XRD, CuKα radiation; λ = 0.15414 nm) at the scan rate of 2° min^{-1} in the 2θ range of 5 and 80°. Scanning electron microscopy (SEM) was performed using JSM-6700F (field emission gun; specimen chamber pressure of about 10^{-5} Pa; accelerating voltage 10 kV; working distance 8 mm). Transmission electron microscopy (TEM, JEM-2010F; 200 keV) was used to study the morphology and microstructure of the composites. Raman spectrum measurements were carried out using INVIA (RENISHAW, England) system with a 514.5 nm wavelength incident laser light. X-ray photoelectron spectroscopy (XPS) analysis was performed using a Kratos AXIS Ultra DLD XPS equipped with a 180° hemispherical energy analyzer. Photoelectron was stimulated by monochromated Al Kα radiation (1486.6 eV) with an operating power of 150 W. It was operated in the analyzer mode at 80 eV for survey scans and 20 eV for detailed scans of core level lines.

Electrochemical characterization. Electrochemical experiments were performed using 2032 coin-type cells. The working electrode consisted of 85 wt.% active material, 10 wt.% carbon black and 5 wt.% polytetrafluoroethylene (PTFE) binder. The electrolyte was a solution of 1 M $LiPF_6$ in EC/DEC (1 : 1 by weight) (purchased from Zhangjiagang Guotai-Huarong New Chemical Materials Co. Ltd). Pure Li foil was used as the counter electrode and Celgard 2300 was used as the separator. In a typical measurement, cyclic voltammetry (CV) was done between 2.0 and 4.2 V (except indicated separately) at a scan rate of 0.1 mV/s by CHI650A (Shanghai CH Instrument Company, China). In the charging/discharging measurement, the cells were charged in a constant current mode to 4.2 V and then continued to be charged in a constant voltage mode at 4.2 V until the current reached 0.05 C; following were discharged in a constant current mode to 2.0 V at room temperature using a battery tester (Land, China).

1. Jeong, G., Kim, Y.-U., Kim, H., Kim, Y.-J. & Sohn, H.-J. Prospective materials and applications for Li secondary batteries. *Energ. Environ. Sci.* **4**, 1986–2002 (2011).
2. Tarascon, J. M. & Armand, M. Issues and challenges facing rechargeable lithium batteries. *Nature* **414**, 359–367 (2001).
3. Thackeray, M. M., Wolverton, C. & Isaacs, E. D. Electrical energy storage for transportation-approaching the limits of, and going beyond, lithium-ion batteries. *Energ. Environ. Sci.* **5**, 7854–7863 (2012).
4. Wang, L., Tang, Z., Ma, L. & Zhang, X. High-rate cathode based on $Li_3V_2(PO_4)_3$/C composite material prepared via a glycine-assisted sol–gel method. *Electrochem. Commun.* **13**, 1233–1235 (2011).
5. Qiao, Y. Q. *et al.* Synthesis and improved electrochemical performances of porous $Li_3V_2(PO_4)_3$/C spheres as cathode material for lithium-ion batteries. *J. Power Sources* **196**, 7715–7720 (2011).
6. Zhang, L. *et al.* $Li_3V_2(PO_4)_3$@C/graphene composite with improved cycling performance as cathode material for lithium-ion batteries. *Electrochim. Acta* **91**, 108–113 (2013).
7. Su, F.-Y. *et al.* Flexible and planar graphene conductive additives for lithium-ion batteries. *J. Mater. Chem.* **20**, 9644–9650 (2010).
8. Williams, G., Seger, B. & Kamat, P. V. TiO_2-graphene nanocomposites. UV-assisted photocatalytic reduction of graphene oxide. *ACS Nano* **2**, 1487–1491 (2008).
9. Rui, X. H., Ding, N., Liu, J., Li, C. & Chen, C. H. Analysis of the chemical diffusion coefficient of lithium ions in $Li_3V_2(PO_4)_3$ cathode material. *Electrochim. Acta* **55**, 2384–2390 (2010).
10. Dominko, R. *et al.* Impact of the carbon coating thickness on the electrochemical performance of $LiFePO_4$/C composites. *J. Electrochem. Soc.* **152**, A607–A610 (2005).
11. Huang, H., Yin, S. C., Kerr, T., Taylor, N. & Nazar, L. F. Nanostructured composites: a high capacity, fast rate $Li_3V_2(PO_4)_3$/Carbon cathode for rechargeable lithium batteries. *Adv. Mater.* **14**, 1525–1528 (2002).
12. Ren, M. M., Zhou, Z., Gao, X. P., Peng, W. X. & Wei, J. P. Core−Shell $Li_3V_2(PO_4)_3$@C composites as cathode materials for lithium-ion batteries. *J. Phys. Chem. C* **112**, 5689–5693 (2008).
13. Dikin, D. A. *et al.* Preparation and characterization of graphene oxide paper. *Nature* **448**, 457–460 (2007).
14. Lee, C., Wei, X., Kysar, J. W. & Hone, J. Measurement of the elastic properties and intrinsic strength of monolayer graphene. *Science* **321**, 385–388 (2008).
15. Hu, L. H., Wu, F. Y., Lin, C. T., Khlobystov, A. N. & Li, L. J. Graphene-modified $LiFePO_4$ cathode for lithium ion battery beyond theoretical capacity. *Nat. Commun.* **4**, 1–7 (2013).
16. Liu, H., Gao, P., Fang, J. & Yang, G. $Li_3V_2(PO_4)_3$/graphene nanocomposites as cathode material for lithium ion batteries. *Chem. Commun.* **47**, 9110–9112 (2011).
17. Pan, A. *et al.* Nano-structured $Li_3V_2(PO_4)_3$/carbon composite for high-rate lithium-ion batteries. *Electrochem. Commun.* **12**, 1674–1677 (2010).
18. Pei, B., Jiang, Z., Zhang, W., Yang, Z. & Manthiram, A. Nanostructured $Li_3V_2(PO_4)_3$ cathode supported on reduced graphene oxide for lithium-ion batteries. *J. Power Sources* **239**, 475–482 (2013).
19. Choucair, M., Thordarson, P. & Stride, J. A. Gram-scale production of graphene based on solvothermal synthesis and sonication. *Nat. Nanotechnol.* **4**, 30–33 (2009).
20. Zhu, X. J., Liu, Y. X., Geng, L. M. & Chen, L. B. Synthesis and performance of lithium vanadium phosphate as cathode materials for lithium ion batteries by a sol-gel method. *J. Power Sources* **184**, 578–582 (2008).
21. Liu, H. *et al.* Kinetics of conventional carbon coated-$Li_3V_2(PO_4)_3$ and nanocomposite $Li_3V_2(PO_4)_3$/graphene as cathode materials for lithium ion batteries. *J. Mater. Chem.* **22**, 11039–11047 (2012).
22. Zhu, X. J., Zhu, Y. W., Murali, S., Stollers, M. D. & Ruoff, R. S. Nanostructured reduced graphene oxide/Fe_2O_3 composite as a high-performance anode material for lithium ion batteries. *Acs Nano* **5**, 3333–3338 (2011).
23. Yin, S. C., Grondey, H., Strobel, P., Anne, M. & Nazar, L. F. Electrochemical property: structure relationships in monoclinic $Li_{3-y}V_2(PO_4)_3$. *J. Am. Chem. Soc.* **125**, 10402–10411 (2003).

Acknowledgments

This work was supported by the Natural Science Foundation of Hubei Province (No. 2011CDB161). H.Ji thanks the support from 100 Talents Program of Chinese Academy of Sciences, and USTC Startup. Y. Zhu thanks the support from China Government 1000Plan

Talent Program, China MOE NCET Program, NSFC Program (51322204) and the Fundamental Research Funds for the Central Universities (WK2060140014).

Author contributions

H.Z., W.W., Y.Z. and Z.Y. conducted the experimental parts. W.Z. and Y.D. contributed to the characterization processes. H.J. carried out data analysis. X.Z., H.J. and Y.Z. designed the experiment and wrote the manuscript. All authors reviewed the manuscript.

Additional information

Supplementary information accompanies this paper at http://www.nature.com/scientificreports

Competing financial interests: The authors declare no competing financial interests.

How to cite this article: Zhu, X.J. *et al*. Manipulating Size of $Li_3V_2(PO_4)_3$ with Reduced Graphene Oxide: towards High-Performance Composite Cathode for Lithium Ion Batteries. *Sci. Rep.* **4**, 5768; DOI:10.1038/srep05768 (2014).